# Dissolved iron in the Arctic Ocean: Important role of hydrothermal sources, shelf input and scavenging removal

M. B. Klunder,[1] P. Laan,[1] R. Middag,[1,2] H. J. W. de Baar,[1,3] and K. Bakker[4]

Received 17 March 2011; revised 20 January 2012; accepted 22 January 2012; published 7 April 2012.

[1] Arctic Ocean waters exchange with the North Atlantic, and thus dissolved iron (DFe) in the Arctic has implications for the global Fe cycle. We present deep water (>250 m) DFe concentrations of the Central Arctic Ocean (Nansen, Amundsen and Makarov Basins). The DFe concentration in the deep waters varies considerably between these basins, with the lowest DFe concentrations (0.2–0.4 nM) in the Makarov Basin, higher concentrations (∼0.45 nM) in the Amundsen Basin and highest concentrations (∼0.6–0.7 nM) in the Nansen Basin. Atlantic input from the shelf seas and slopes enhances the DFe concentration in the Nansen Basin. Moreover, hydrothermal activity at the Gakkel Ridge causes a significant and widespread enrichment of DFe in the Eurasian Basins, at a depth of 2000–3000 m. Below this maximum, the important role of scavenging and absence of input sources are reflected in a strong relation with dissolved Mn (DMn) and in very low (<0.25 nM) DFe concentrations in the deepest (>3000 m) Amundsen and Makarov Basins. The depth profiles of DFe in the Arctic Ocean, notably in the Makarov Basin, deviate from the DFe distribution pattern observed in other parts of the world ocean.

**Citation:** Klunder, M. B., P. Laan, R. Middag, H. J. W. de Baar, and K. Bakker (2012), Dissolved iron in the Arctic Ocean: Important role of hydrothermal sources, shelf input and scavenging removal, *J. Geophys. Res.*, *117*, C04014, doi:10.1029/2011JC007135.

## 1. Introduction

[2] The trace metal iron (Fe) is an important factor in biogeochemical cycles of the world ocean via its control of phytoplankton growth [*Martin and Gordon*, 1988; *de Baar et al.*, 1995; *Bruland et al.*, 1995; *Boyd et al.*, 2000; *Turner and Hunter*, 2001] and is therefore of major importance for marine ecosystems. In recent decades, major advances have been made in understanding the role of Fe in global marine biogeochemical cycles [*de Baar and de Jong*, 2001; *Gregg et al.*, 2003; *Parekh et al.*, 2004]. However, due to harsh conditions, data on trace metal concentrations in the Arctic Ocean are scarce [e.g., *Measures et al.*, 1999; *Middag et al.*, 2009], in particular for deep waters. To the best of our knowledge, it is restricted to one vertical profile of DFe (<0.4 $\mu$m) concentrations in Baffin Bay, west of our study area, with DFe concentrations in the 4.5–11 nM range [*Campbell and Yeats*, 1982] and recently *Nakayama et al.* [2011] reported DFe data from the Canada Basin and Chukchi shelf. However, the Arctic region is of importance in understanding the global distribution of trace metals, such as Fe. The deep waters of the Arctic Ocean are linked with the North Atlantic Ocean, renewing North Atlantic Deep Water (NADW) [*Rudels et al.*, 2005], which has been shown to play an important role in the Fe cycle in the Atlantic Ocean [*Laës et al.*, 2003; *Sarthou et al.*, 2007] and Southern Ocean [*Klunder et al.*, 2011; *Chever et al.*, 2010]. Moreover, the major role of iron in nitrogen fixation raises the question whether the iron flux from the Arctic provides the increase in DFe in the Atlantic which is necessary for nitrogen fixation rates [*Arrigo et al.*, 2008].

[3] Hydrothermal vents have been shown to be an important source of (dissolved) Fe in the deep world ocean [*Klinkhammer et al.*, 2001; *Tagliabue et al.*, 2010; *Klunder et al.*, 2012; *Wu et al.*, 2011]. Active vents have been identified above the Gakkel Ridge [*Edmonds et al.*, 2003]. These vents could be an important input source for DFe in the deep Arctic Ocean. Another possible input source of DFe is dissolution of resuspended particles originated from continental shelves. The transport of DFe from shelf regions to deep waters has been reported in the North Atlantic Ocean [*Laës et al.*, 2007], North Pacific Ocean [*Elrod et al.*, 2004; *Lam and Bishop*, 2008], and around islands in the Southern Ocean [*Ardelan et al.*, 2010; *Bucciarelli et al.*, 2001]. The DFe input by shelf sediments may be even more important in the Arctic as shallow shelf seas comprise roughly one third of the Arctic Ocean. The relatively large number of particles transported from rivers and shelf seas to the deep basins may

[1]Biological Oceanography, Royal Netherlands Institute for Sea Research, Den Burg, Netherlands.
[2]Department of Ocean Sciences and Institute of Marine Sciences, University of California, Santa Cruz, California, USA.
[3]Department of Ocean Ecosystems, Rijksuniversiteit Groningen, Groningen, Netherlands.
[4]Geological Oceanography, Royal Netherlands Institute for Sea Research, Den Burg, Netherlands.


0148-0227/12/2011JC007135

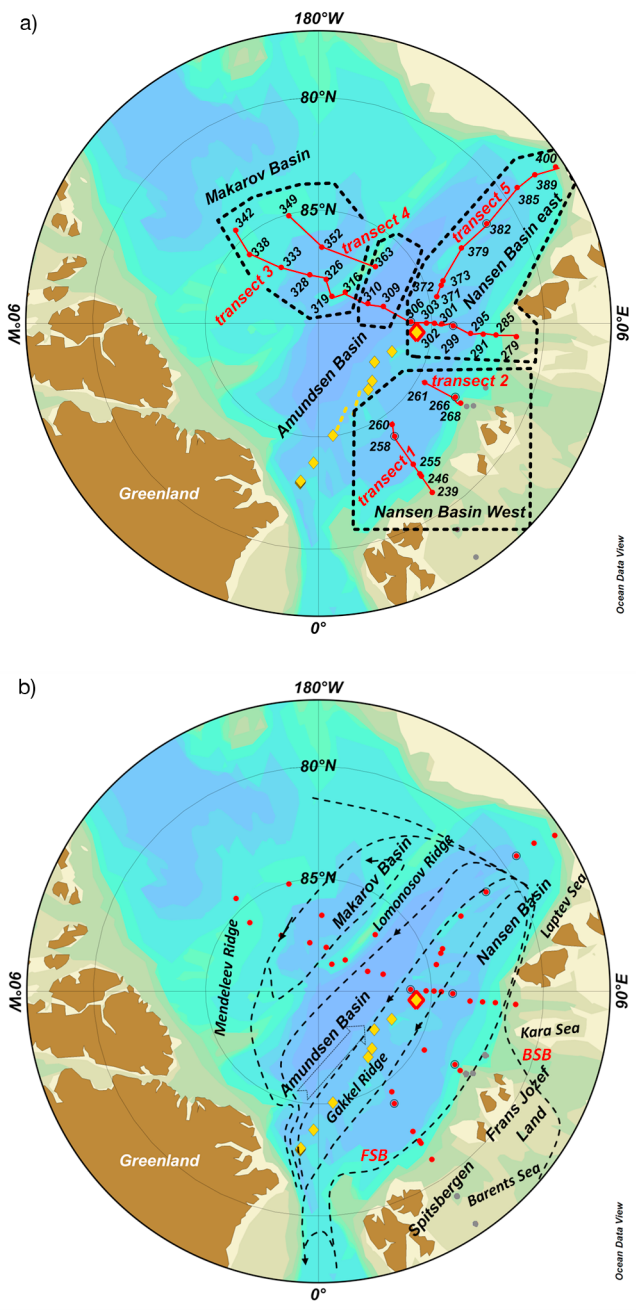


**Figure 1.** Chart of the Central Arctic Ocean, including the stations occupied during ARK XXII/2. Sampling stations for DFe are indicated (red dots) and in Figure 1a station number is annotated. Gray dots represent stations which are described by *Klunder et al.* [2012]. (a) Four different regions are indicated by a black dotted line. Hydrothermal vents as reported by *Edmonds et al.* [2003] are shown as yellow diamonds. Largest diamond (red-yellow) shows the vent used for calculation in Figure 10. (b) Flow directions [after *Jones et al.*, 1995] are indicated. Dotted arrow indicates deep (>2000 m) currents as proposed by *Jones et al.* [1995]. Indicated in red are the different branches of Atlantic water (FSB, Fram Strait Branch; BSB, Barents Sea Branch). This figure was created using Ocean Data View [*Schlitzer*, 2002].

shift the balance between organic complexation and scavenging removal [*Wu et al.*, 2001] and allow DFe to be scavenged out of the deep waters, resulting in relatively low concentrations for deep water.

[4] Within the framework of the international IPY-GEOTRACES program trace metals were measured during a cruise in the Arctic Ocean. This paper describes the cycle of DFe in the deep Arctic Ocean. The distribution of DFe in the Arctic Shelf seas and surface waters can be found in the complementary manuscript [*Klunder et al.*, 2012].

## 2. Materials and Methods

### 2.1. Sampling and Analysis

[5] Seawater samples were collected during the ARK XXII/2 expedition of the RV *Polarstern* between 1 August and 23 September 2007. Sampling stations were located in the Eurasian and Canada Basins; the cruise track is depicted in Figure 1. At discrete depths, samples were collected using 24 internal Teflon coated PVC GO-FLO Samplers (12 L; General Oceanics Inc.) mounted on a Titanium frame (Ultraclean frame) which was connected to a Kevlar hydrowire with internal signal cables and controlled from aboard [*de Baar et al.*, 2008]. The samples for iron analysis were collected from the GO-FLO bottles in a class 100 clean room environment [*de Baar et al.*, 2008]. Seawater was filtered through a 0.2 $\mu$m filter cartridge (Sartrobran-300, Sartorius) under nitrogen pressure (1.5 atm.). For each depth replicate samples of dissolved iron were taken in 60 ml LDPE sample bottles and acidified to pH = 1.8 with 12 M HCl (Baseline, Seastar Chemicals). All bottles, used for storage of reagents and samples, were previously acid cleaned according to a three step cleaning procedure as described by *Middag et al.* [2009].

[6] Dissolved Fe was measured using flow injection analysis with luminol chemiluminescence, where samples were buffered in-line to pH = 4, using a 0.12 M ammonium acetate buffer (pH = 6.5). The Fe was pre-concentrated on an IDA Toyopearl AF-Chelate resin [*Klunder et al.*, 2011]. After pre-concentration, the column was rinsed (60 s) with de-ionized ultrapure (DI) water (18.2 MΩ) and Fe was eluted from the column (120 s) using 0.4 M HCl (Merck Suprapur) [*Klunder et al.*, 2011]. Subsequently, this mixture was mixed (in a 1 m mixing coil at 35°C) with 0.96 M $NH_4OH$ and 0.5 M $H_2O_2$ (Merck Suprapur) and 0.3 mM luminol (with 0.7 mM TETA) (Sigma chemicals). Pre-concentration time was usually 120 s, except for the Laptev Sea stations, where a short loading time (15 s) enabled detection of the very high concentrations present at this location.

### 2.2. Calibration and Validation

[7] The system was calibrated by standard additions of DFe (range 0.15–3 nM) to low DFe seawater. Initially filtered seawater from an earlier cruise (North Atlantic Ocean, water depth of chl a maximum) was used as calibration water, during the cruise new seawater from the depth of the chl a maximum was used. Generally, calibration water contained <∼0.2 nM DFe. When an outlying value was suspected for DFe, profiles of Al, Mn, and nutrients were considered to evaluate the consistency of the data point in question. In case no deviations were observed in the other parameters and both the initial and duplicate sample showed

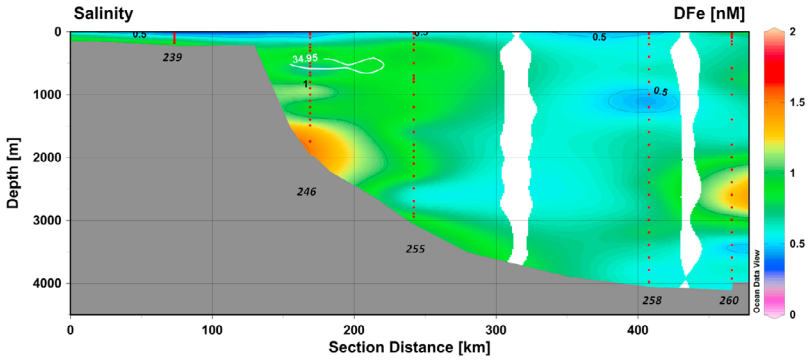


**Figure 2.** Color plot of concentrations of dissolved Fe (nM) for transect 1 (see Figure 1a). Red dots indicate sample points. Station numbers are mentioned below the transect. White contour lines indicate a salinity of 34.95. This figure was created using Ocean Data View [*Schlitzer*, 2002].

an the exceptional value, the deviation in Fe-concentration was calculated, based on the values below and above. Briefly, the suspected outlying data point was considered as erroneous (likely due to contamination of the sample) in case the value positively deviated more than +25% from this calculated "expected" profile based on the Fe-concentration above and below the data point [after *Middag et al.*, 2009]. The total number of data points for Fe during ARK XXII/2 was 785. In total five data points were rejected, of which three were situated in the deeper waters discussed in this manuscript. Data Set S1 including stations positions, date, depth, nutrient data, DFe data, and total alkalinity is available in the auxiliary material.[1] The blank, the background concentration of DFe in DI water and chemicals, defined as the amount of photons measured when not loading any seawater onto the column, was 0.02 ± 0.02 nM ($n$ = 41) on average and did not exceed 0.075 nM. The detection limit ($3\sigma$ of the blank) was 0.07 nmol $l^{-1}$. The amount of DFe added to the sample by addition of the equivalent of 2 ml 12 M HCl (Baseline, Seastar) per liter is <3 pmol per sample; this is deemed negligible [*Klunder et al.*, 2011]. The accuracy of the Fe Flow injection analysis system was verified by regularly analyzing SAFe D2 standard seawater. The results agreed well with the community consensus values: 0.92 ± 0.057 nM, $n$ = 24. (Reported values are 0.92 ± 0.03 (http://www.geotraces.org).)

### 2.3. Other Parameters

[8] Dissolved manganese (DMn) and aluminum (DAl) were simultaneously sampled with DFe [*Middag et al.*, 2009, 2011]. Moreover, at selected stations Fe was measured in different size fractions; a non filtered fraction giving the total dissolvable Fe (TDFe) concentration (measured after 1 year dark storage [*Thuróczy et al.*, 2011]), and an ultra-filtrated fraction, giving the Fe fraction smaller than 1000 kDa. These results as well as the organic complexation of Fe in the three size fractions are reported by *Thuróczy et al.* [2011]. Data of salinity and potential temperature were taken from the Ultraclean CTD. As an indication of particle concentration and presence, mostly light transmission data from the regular CTD is used, this CTD is deployed (by Alfred Wegener Institute) at the same stations just after the Ultraclean CTD deployment. At stations where no light transmission data were available, turbidity, from the turbidity sensor on the Ultraclean-CTD, is presented. Nutrient data was measured from hydrocasts with the Ultraclean frame and regular hydrocasts, as described by *Middag et al.* [2009].

## 3. Hydrography

[9] Several transects were sampled from the extensive shelf waters into the Arctic Ocean's interior, of which the third and fourth transect extended as far east as the Mendeleev Ridge (Figure 1a). The main source of water in the Arctic Ocean interior is surface and intermediate water flowing in from the North Atlantic Ocean (Figure 1b). In the Arctic Ocean, the surface waters consist of the upper Polar Mixed Layer, freshened by ice-melt and outflow from the shelves. A strong, well defined halocline is found below the upper Polar Mixed Layer [*Rudels*, 2001]. The close to freezing temperatures yet strong salinity gradient with depth in the halocline prevents vertical mixing, which implies advective sources for the halocline waters above the Atlantic Waters [*Rudels*, 2001].

[10] Below the halocline waters, Atlantic and intermediate waters are observed. These Atlantic waters form a boundary current, along the continental shelves in the Arctic Ocean [*Rudels et al.*, 2000]. This inflowing Atlantic water has two branches; the first one, almost unmodified warm, saline Atlantic water flows through Fram Strait (Fram Strait Branch (FSB)) following the Eurasian Basin slope. The second branch flows over the extended shelves of the Barents Sea (Barents Sea Branch (BSB)), where it is modified by brine-enriched shelf water (Figure 1b). Incorporation of freshwater from ice melt and terrestrial runoff to the Barents Sea causes the Barents Sea branch end-member to be colder and less saline than the Fram Strait branch. *Schauer et al.* [1997, 2002] reported the inflow of BSB to the basin at depths between 200 and 1300 m and that this water is slightly less saline than the overlying Fram Strait Branch Water. *Ekwurzel et al.* [2001] defined Atlantic Water as water with salinity >34.9 and potential temperature ($\theta$) >3°C, although it gets colder and fresher during the transit through Fram Strait or over the Barents Sea shelf. During our cruise only very few data points

[1]Auxiliary materials are available at ftp://ftp.agu.org/apend/jc/2011JC007135.

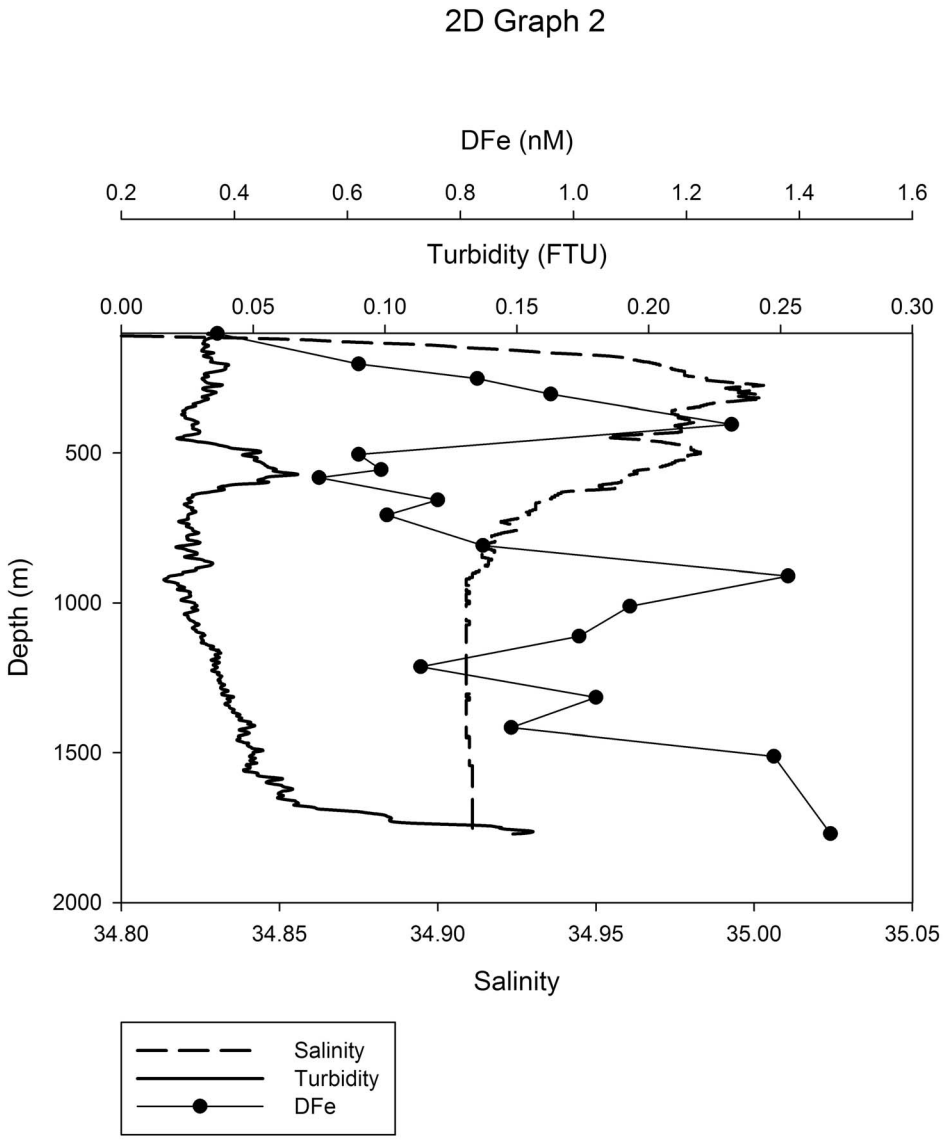


**Figure 3a.** Concentration of DFe (nM) and salinity profile of station 246 (Barents Sea Slope). Turbidity is also indicated in arbitrary units, indicative of particle concentration in the water.

showed a $\theta > 3°C$ [*Middag et al.*, 2009] but a salinity maximum of >34.95 was observed at transect 1, 2 and 3 (Figure 2). Due to mixing with low salinity waters this maximum was not observed at transect 5. Upon mixing, the boundary current follows a counterclockwise circulation, with a branch flowing along the Gakkel Ridge back to Fram Strait, a branch following the Lomonosov Ridge, and a branch crossing the Lomonosov Ridge and entering the Makarov basin (Figure 1b). The latter branch is largely influenced by sea-ice formation, brine rejection (i.e., increasing salinity) and subsequent formation and convection of dense water along the slopes, causing the Canada Basin to be strongly influenced by shelf waters. This influence of slope convection causes the Canada Basin Deep Water (CBDW) to be less cold and relatively saline compared to Eurasian Basin Deep Water (EBDW) [*Rudels*, 2001]. During this study the EBDW was observed in the Nansen and Amundsen Basins and defined as the deep ($S > 34.8$) waters with $\theta < -0.8°C$ and the CBDW as the deep waters with $\theta < -0.4°C$ [after *Middag et al.*, 2009]. In this study, the CBDW observed in the Makarov Basin is named Makarov Basin Deep Water (MBDW). Finally, Atlantic and intermediate waters are defined as those waters with $\theta > -0.8°C$ which are not part of the surface waters [after *Middag et al.*, 2009].

## 4. Results

### 4.1. Transects 1 and 2

[11] This paper focuses on the concentrations of DFe in the deep waters of the Arctic Ocean, and does not include shelf stations along transect 1 and 2 (Figure 1). For shelf and upper water column DFe values see the companion [*Klunder et al.*, 2012].

[12] Above the continental slope of the Barents Sea, in general relatively high DFe value's of ~0.9–1.0 nM were

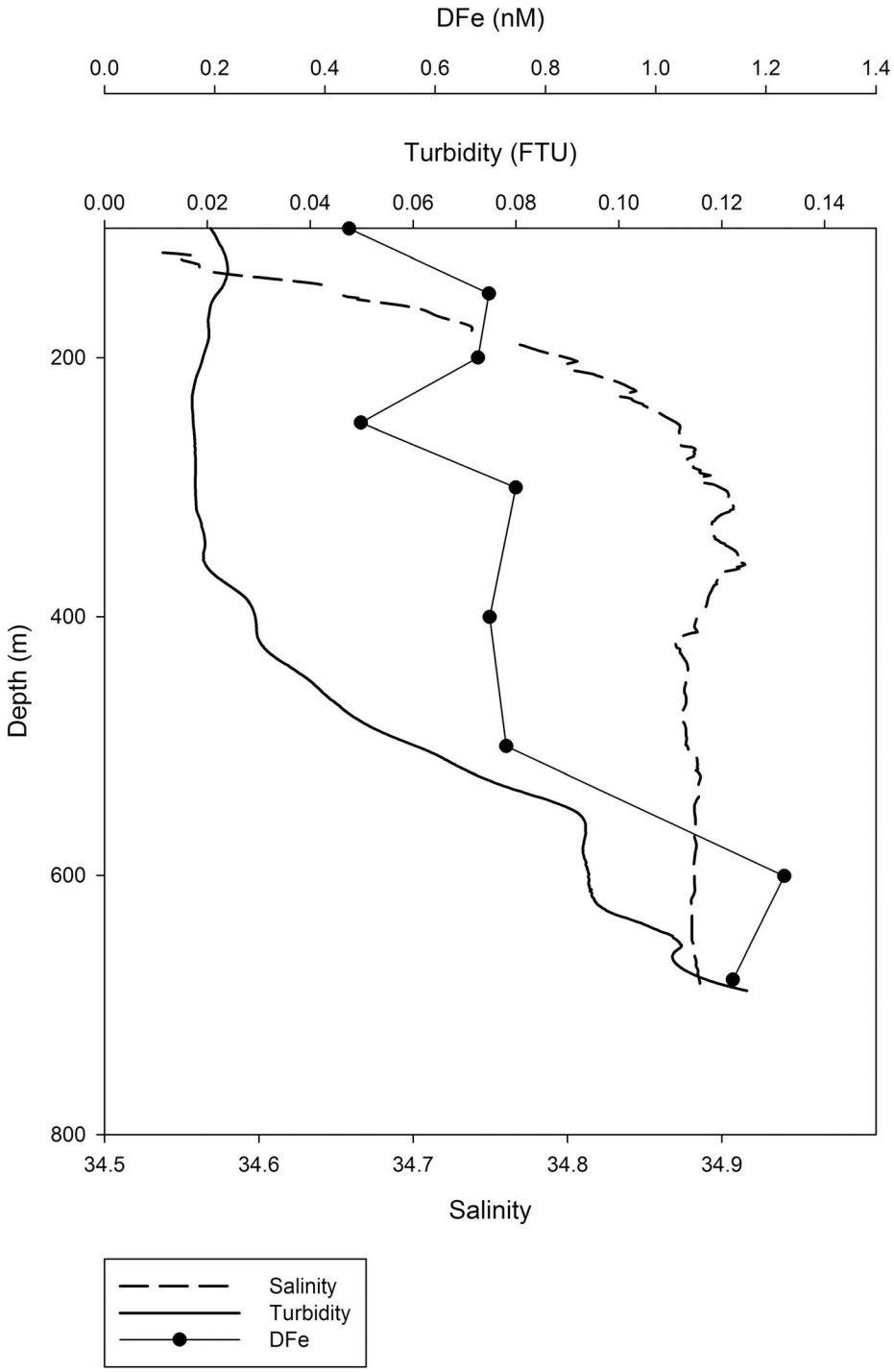


**Figure 3b.** Concentration of DFe (nM) and salinity profile of station 285 (Kara Sea Slope). Turbidity is also indicated in arbitrary units, indicative of particle concentration in the water.

observed from ~200 m downward, with very high values at ~400 m, at ~1000 m, and close to the bottom (~2000 m) (Figures 2, 3a–3c, and 4). The inflow of the Atlantic boundary layer was identified in the salinity, consistent with anomalies in the potential temperature ($\theta$) (not shown) and turbidity profiles at ~500–800 m depth (Figure 3a). Here, the DFe concentration decreased to ~0.7 nM, a typical concentration for (unmodified) Atlantic waters [*Moore and Braucher*, 2008].

[13] Three stations were sampled in the Nansen Basin at transect 2. These three stations are not sufficient to make a contour plot and the DFe distribution is thus depicted as a depth profile in Figure 5. Concentrations of DFe were relatively constant at 0.4–0.5 nM at ~500 m. From 700 m to the

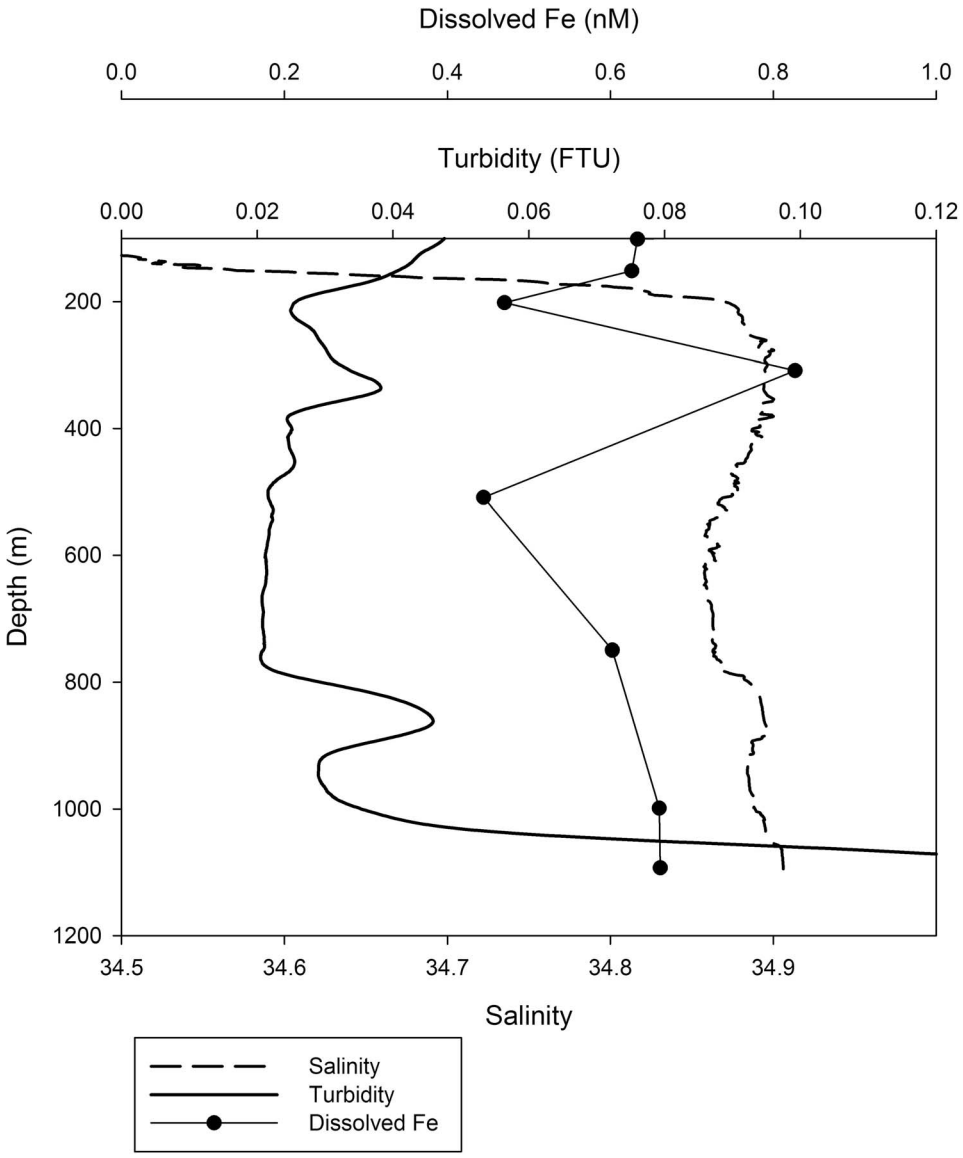


**Figure 3c.** Concentration of DFe (nM) of station 400 (Laptev Sea Slope). Turbidity is also indicated in arbitrary units, indicative of particle concentration in the water.

bottom, concentrations increased to 0.6–0.8 nM. In the upper 1000 m in the center of the Basin, there was a difference between the two transects; higher DFe (∼0.7 nM) was observed in the western part (transect 1), whereas lower DFe concentrations (<0.5 nM) were observed further eastward (transect 2) (Figures 2 and 5). Below 1000 m, concentrations increased to a very pronounced maximum with DFe concentrations ∼1.3 nM at transect 1 and ∼0.8 nM at transect 2. Moreover, at transect 2, two separate maxima were observed at ∼2250 and 3200 m. At both transects, concentrations decreased toward the bottom below the maxima.

### 4.2. Transect 3

[14] Concentrations <0.5 nM were observed in the upper 1000 m of transect 3, throughout all basins (Figure 6). Slightly higher (0.5–1 nM) concentrations were found above the shelf and slope of the Nansen Basin. An intrusion of high DFe (>1 nM) concentrations was observed from the Kara Sea shelf into the Basin just below the Atlantic water, at 750 m depth, consistent with a lower light transmission signal observed between 400 and 800 m (Figure 3b) indicating a relatively high particle concentration.

[15] A similar intrusion was observed slightly deeper below 1200 m depth with a small peak in DFe at ∼1700 m, which shifts to ∼1500 m depth further into the basin. This peak in the concentration of DFe is highest (from 0.61 to 0.84 nM) at the station closest to the shelf (station 291), where a similar maximum was observed in the depth profile of DMn concentrations [*Middag et al.*, 2011]. At station 299 this maximum was much less pronounced for the concentration of DFe and disappeared fully for DMn [*Middag et al.*,

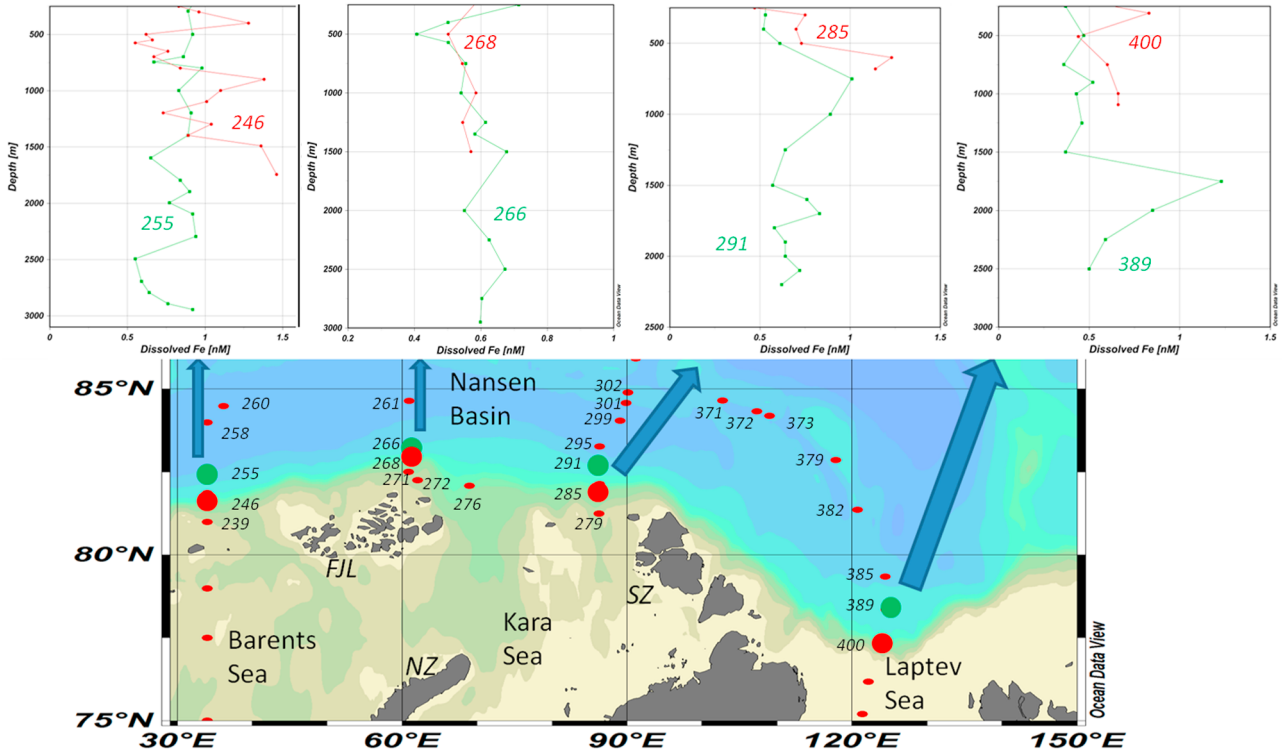


**Figure 4.** Dissolved Fe depth profiles of slope stations (bottom depth <3000 m). Station numbers are indicated. FJL, Frans Jozef Land; NZ, Nova Zemlya; SZ, Svernaya Zemlya. This figure was created using Ocean Data View [*Schlitzer*, 2002].

2011]. A very pronounced DFe maximum of 1.71 nM was situated around 2500–3000 m depth above the Gakkel Ridge (Figure 6, station 306). This maximum in DFe influenced the deepest waters (>2000 m) of the Nansen Basin and, although less pronounced, the waters at 2000–3000 m in the Amundsen and Makarov Basins (Figure 6).

[16] In the Amundsen Basin, the background concentrations of DFe were in general <0.5 nM, but concentrations reaching ~0.7 nM were observed at 2000–2500 m depth. Slightly higher DFe concentrations were found above the Lomonosov Ridge, and the concentrations of DFe decreased again to very low concentrations <0.3 nM in the deep Makarov Basin waters (Figure 6).

### 4.3. Transect 4

[17] The fourth transect comprises three stations situated on the Mendeleev Ridge (349), in the Makarov Basin (352) and over the Lomonosov Ridge (363), respectively. These stations are too far apart to show in a contour plot; therefore the vertical profiles are shown (Figure 7). At all stations the high DFe concentrations in the surface decreased to relatively constant concentrations (0.3–0.5 nM) between 200 and 500 m depth. Enhanced DFe concentrations (~0.8 nM) were observed at 1000 m and 1750 m above the Lomonosov Ridge. In the Makarov Basin, a maximum in the DFe concentration was observed at 1000 m, changing the trend of decreasing DFe with depth. In contrast, the Amundsen Basin stations showed a (slightly) increasing trend with depth between 1000 and 2000 m. Below 2000 m, a maximum at 2250 m and a very low concentration at 2750 m were observed at both stations. Below 1500 m depth, the station in the Makarov Basin showed a constant ~0.1–0.15 nM lower concentration compared to the Amundsen Basin.

### 4.4. Transect 5

[18] The fifth and last transect starts above the Nansen Gakkel Ridge approximately 0.6° southward and 12°

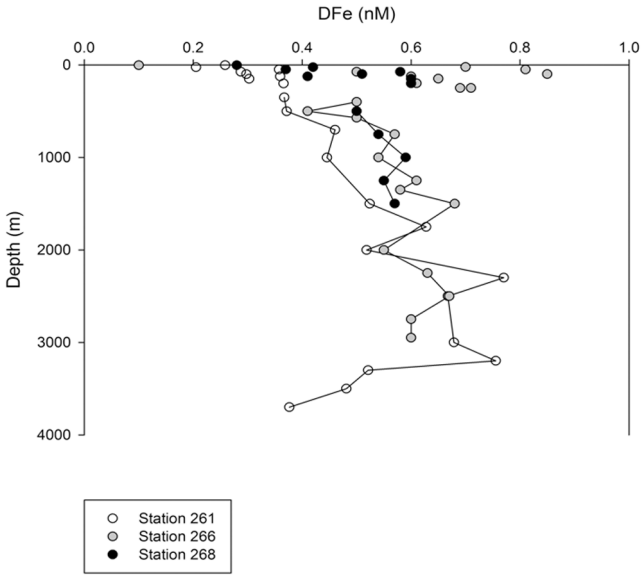


**Figure 5.** Depth profiles of concentrations of dissolved Fe (nM) for all open ocean stations of transect 2. For clarity, connector line of the upper 1000 m is excluded.

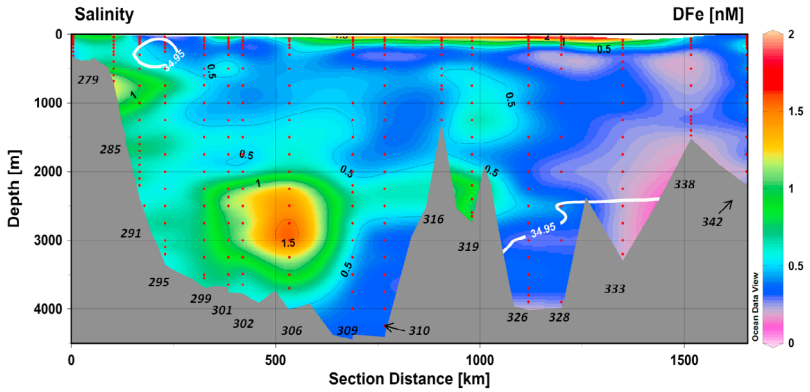


**Figure 6.** Color plot of concentrations of dissolved Fe (nM) for transect 3 (see Figure 1a). Red dots indicate sample points. Station numbers are mentioned below the transect. White contour lines indicate a salinity of 34.95. Basins: Nansen Basin at 100–500 km, Amundsen Basin at 500–800 km, and Makarov Basin at 1100–1500 km. Ridges: Gakkel Ridge at ~500 km, Lomonosov Ridge at ~800–1100 km, and Alpha Ridge at ~1500 km. This figure was created using Ocean Data View [*Schlitzer*, 2002].

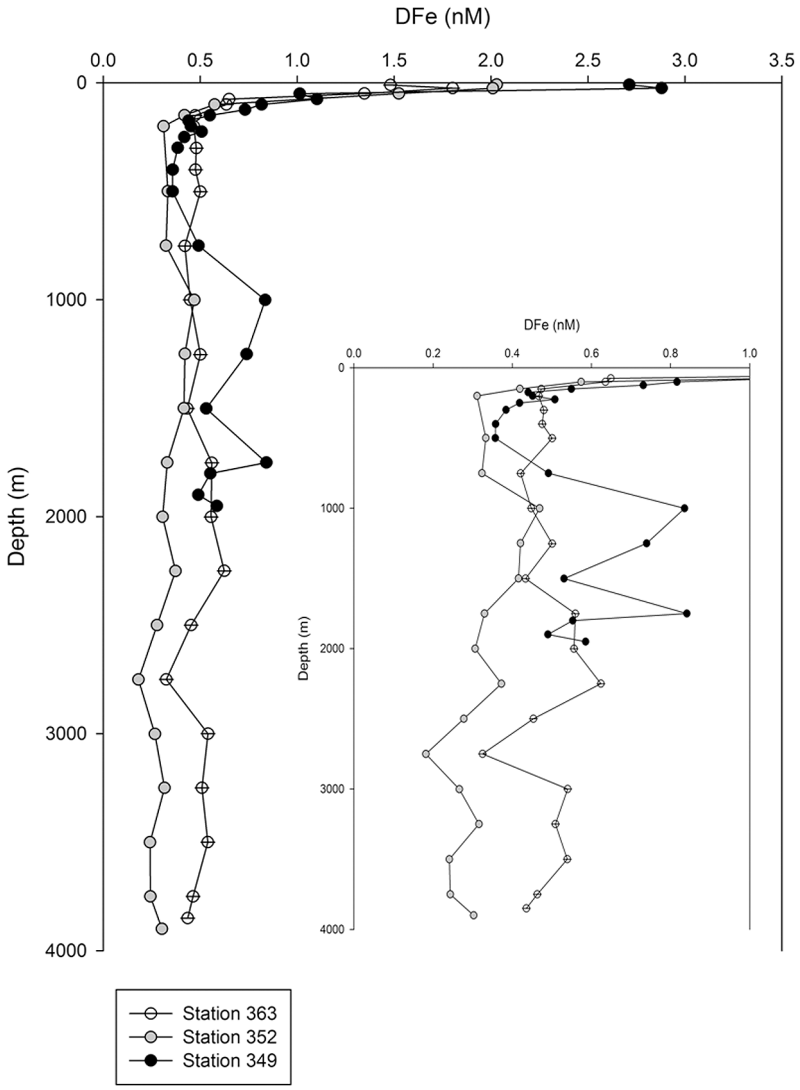


**Figure 7.** Depth profiles of dissolved Fe for all open ocean stations of transect 4. The inset shows DFe at a 1 nM scale.

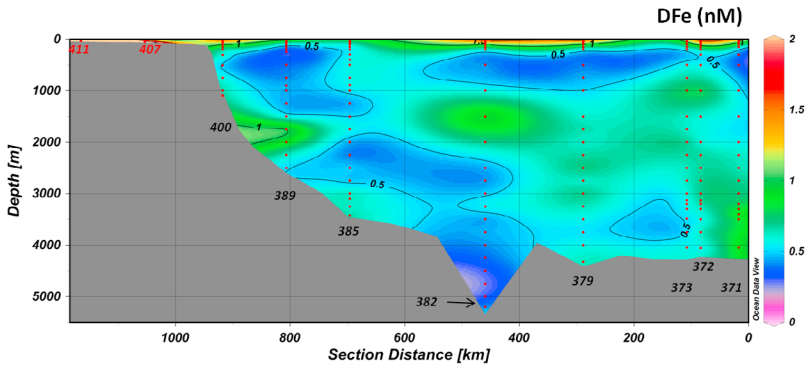


**Figure 8.** Color plot of concentrations of dissolved Fe (DFe, nM) for transect 5 (see Figure 1a). Red dots indicate sample points. Station numbers are mentioned below the transect. Station numbers in red are not discussed in this manuscript but by *Klunder et al*. [2012]. White contour lines indicate a salinity of 34.95. This figure was created using Ocean Data View [*Schlitzer*, 2002].

eastward from the crossing of the Gakkel Ridge of transect 3 (Figure 1). From here it follows a southeastward direction, along the Gakkel Ridge, Nansen Basin, Laptev Sea slope and the final station was located above the shelve of the Laptev Sea (<100 m depth). Figure 8 shows the DFe concentrations over transect 5. In general, the DFe concentration in the Deep Nansen Basin above the Gakkel Ridge was ~0.6 nM. The elevated concentrations, as determined at 2000–2500 m depth within transect 3, were hardly visible in transect 5. However, deeper in the water column, at 3000–3500 m depth, concentrations of DFe were elevated, accompanied by elevated DMn concentrations [*Middag et al.*, 2011] and potential temperature anomalies and transmission anomalies. In the middle of the water column (1000–3000 m depth) concentrations of 0.7–1 nM were observed, whereas above and below these depths, concentrations decrease (Figures 7). An increase of the DFe concentration from the slope into the basin was observed at ~300 and at 1750–2000 m depth (Figures 3c and 4).

## 5. Discussion

### 5.1. Sources and Sinks of Fe in the Arctic Basin

[19] The here observed data for the Nansen, Amundsen and Makarov Basins can be compared with DFe data from the Canada Basin and Chukchi Slope [*Nakayama et al.*, 2011]. Deep waters in the Canada Basin show relatively constant DFe concentrations (~0.5–0.6 nM) similar to deep water concentrations in the Amundsen and Nansen Basins. The stations above the Chukchi slope show higher DFe concentrations (~0.9–1 nM) [*Nakayama et al.*, 2011], similar to shelf influenced DFe concentrations here observed on the Eurasian side of the Arctic Ocean. In this section we discuss the different factors influencing the the distribution of DFe in the Deep Waters of the Arctic Ocean. and give a comparison with DFe distribution in other ocean regions (Figure 9). The concentration of DFe in the Arctic Ocean is determined by the DFe concentration of its contributories (Atlantic and Pacific Water) (see section 5.1.1), in situ mineralization (section 5.1.2), input sources within the Arctic Ocean (advection of shelf derived water, re-suspended sediment (section 5.1.3), hydrothermal sources (section 5.1.4), and export processes (scavenging) and ligand binding and complexation capacity (section 5.1.5).

#### 5.1.1. Interaction With the North Atlantic and North Pacific Oceans

[20] The main contribution of the Arctic Ocean Waters is the inflow of water from the North Atlantic via Fram Strait (FSB) or the Barents Sea (BSB) [*Rudels*, 2001] (Figure 1b; section 3). Slightly higher DFe concentrations (~0.8–0.95 nM) at the depth of the FSB inflow (high $\theta$ and salinity 200–400 m; Figures 2 and 3a) observed at transect 1 indicate high DFe in the Atlantic source waters. Strong geostrophic velocities as reported above the Yarmuk Plateau just north of Spitsbergen [*D'Asaro and Morison*, 1992], may cause particle resuspension. However, because no significant turbidity increase is observed (Figure 3a), this is not very likely, unless dissolution and fast sinking of possible resupended particles have taken place. In general, the closer proximity to Fram Strait (thus Atlantic source) would explain the slightly higher DFe concentrations in the west part of the Nansen Basin compared to the east part (Figures 2, 5, and 9).

[21] Both the intermediate depth layers and the Polar Surface Waters (PSW) exit the Arctic through Fram Strait, west of the Greenwich Meridian [*Rudels et al.*, 2005; *Tanhua et al.*, 2005]. At intermediate depth, this return current is situated close to the Gakkel Ridge (Figure 1b) [*Jones et al.*, 1995] where relatively high Fe was observed. Also DFe-concentrations in PSW were relatively high [*Klunder et al.*, 2011]. These observations indicate that relatively high DFe concentrations are likely present in the Arctic contribution to the Iceland Scotland and Denmark Strait Overflow Waters, and would eventually augment DFe in North Atlantic Deep Water.

[22] In the Makarov Basin, at 2700–3000 m depth, low DFe concentrations were observed as well as distinct phosphate and silicate maxima and a slight salinity minimum. This may reflect downslope convection of waters from the surface, entraining in the deeper waters of the Laptev and Chukchi slopes [*Rudels*, 2001]. Therefore the low DFe concentrations may be caused by either a low Pacific endmember concentration or biological depletion or enhanced scavenging of DFe during transit from the Pacific to the Arctic shelves [*Klunder et al.*, 2011]. As [*Aguilar-Islas*

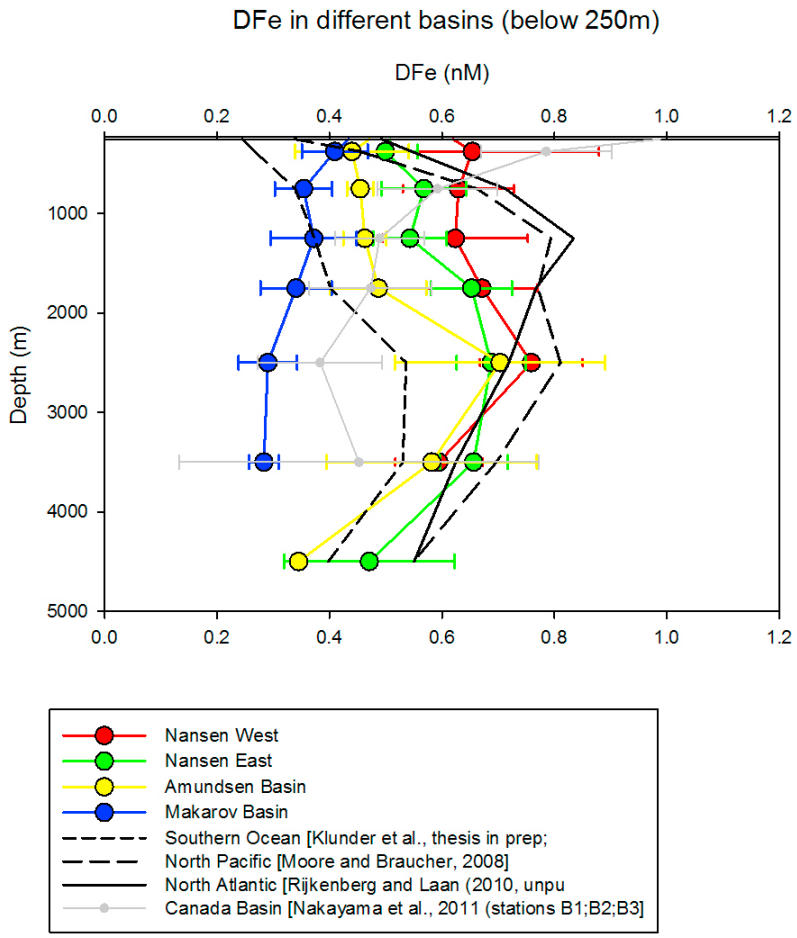


**Figure 9.** Concentrations of DFe (nM) over the different regions in the Arctic Ocean (Figure 1), averaged over depth intervals (250–500, 500–1000, 1000–2000, 2000–3000, 3000–4000, 4000–5000, and 5000–6000 m). Error bars indicate 95% confidence interval. For comparison, similar average values of vertical profiles are shown for the Southern Ocean, North Atlantic, and North Pacific.

*et al.*, 2008] reported DFe-concentrations of 1.21–3.14 nM for North Pacific shelf stations, close to Bering Strait, we do not expect the Pacific source water to be low in DFe. Moreover, the North Pacific water must flow over the Bering Sea Shelf, before reaching Bering Strait. *Aguilar-Islas et al.* [2007] has shown that DFe increases to ~4 nM at the shelf domain. Therefore, biological depletion and/or loss due to scavenging seems to be the more likely cause for the low DFe concentrations [see also *Klunder et al.*, 2011, and references therein].

#### 5.1.2. Remineralization of Exported Biogenic Particles

[23] Remineralization of biogenic particles exported from the mixed layer would theoretically be reflected in a significant (positive) correlation between DFe and major nutrients (silicate(Si), phosphate ($PO_4$) and nitrate and nitrite ($NO_3 + NO_2$). Such a correlation is reported for DFe and ($NO_3 + NO_2$) and for DFe and Si in the North Atlantic Ocean [*Middag*, 2010]. Based on the relationship between Al and Si in the Arctic, *Middag et al.* [2009] concluded that dissolution of biogenic particles (mainly diatoms) must occur in the Atlantic and intermediate layers in the Arctic Ocean. For DFe and Si (or DFe and $NO_3 + NO_2$) however, such a significant (positive) correlation is not observed in the Atlantic and Intermediate waters or in the deep waters of the Arctic Ocean. Moreover, $^{234}Th/^{238}U$ data from the same cruise showed that there was very little export of organic carbon from the upper 100 m to deeper waters in the Arctic Basins [*Cai et al.*, 2010].

[24] This was confirmed by low organic carbon export as determined from $PO_4$ deficit [*Anderson et al.*, 2003] and sediment traps [*Fahl and Nöthig*, 2007]. The $^{234}Th/^{238}U$ ratios integrate the POC export over the preceding 1–2 months, whereas the Al-Si relation reflects processes at longer timescales. Therefore, based on the $^{234}Th/^{238}U$ data and the absence of the relationship between DFe and Si (and DFe and $NO_3 + NO_2$), we expect a relatively low influence of remineralization of organic particles on the DFe input in the intermediate waters of the Arctic Ocean. Also, in the deep waters (MBDW and EBDW), we did not observe a significant positive correlation between DFe and Si (or ($NO_3 + NO_2$)). However, these waters display a strong input of terrestrial material [*Middag et al.*, 2009; *Roeske et al.*, 2012], diminishing a possible biogenic particle remineralisation signal.

#### 5.1.3. Fe Input From Adjacent Shelf Seas and Slopes

[25] Although TDFe concentrations above the Barents and Kara Sea shelves are high (6–60 nM) [*Thuróczy et al.*, 2011], the concentration of dissolved iron does not exceed

that of the slope and open ocean region (0.4–0.54 nM) [*Klunder et al.*, 2012]. The station at transect 1, close to the shelf (station 246) shows a complex pattern of different layers. High potential temperature ($\theta$) and salinity indicate an Atlantic influence at ~200–300 m depth (see section 5.1.1; Figure 2a). There is a thin layer at ~400 m, with low $\theta$ and salinity, where also an enrichment in $\delta^{18}O$ is observed (not shown), all indicative of ice-melt influence [*Ekwurzel et al.*, 2001; *Klunder et al.*, 2012]. Thus, meltwater influenced waters from the shelf may possibly explain the high DFe (1.22 nM) around this depth. Remarkably, the turbidity increase at ~500 m depth, indicative of advective transport form the shelves, does not cause high DFe concentrations but higher DFe concentrations are observed at a smaller turbidity maximum at 900 m depth (Figure 5a). Toward the bottom, elevated DFe, consistent with turbidity (Figure 3a) and elevated Mn [*Middag et al.*, 2011] indicates local resuspension at the slope. There is no sign of advective DFe transport far into the basin, as station 255 does not show enrichement in DFe (Figure 4). Also no advective transport is observed from the shelves into the Basin at transect 2 (Figures 4 and 5). Further east (stations 279–302), in the east part of the Nansen Basin, enrichment with DFe was observed close to the bottom of the Kara Sea slope (Figures 4 and 6). We suggest that the relatively low salinity and high turbidity corresponding to the DFe maximum (Figure 2b) are the result of inflow of BSB water, which picks up particles from the shelf, and then enters the Nansen Basin at a depth of between 500 and 700 m (see section 3.1). Dissolution of Fe from these particles will then be the principal source of DFe. This process has been shown to enhance DFe levels in regions with strong geostrophic velocities, such as the northeast Atlantic [*Laës et al.*, 2007] and above the New Zealand continental shelf [*Croot and Hunter*, 1998]. *D'Asaro and Morison* [1992] and *Schauer et al.* [1997] reported internal wave mixing and eddies in the eastern Nansen Basin, which may have strong enough velocities to cause near-bed mixing and resuspension of sediments.

[26] Dissolution from these particles (>0.2 $\mu$m) during transport from the shelf seas to the slope regions, could cause the maximum in DFe concentration observed in the entire Nansen Basin at ~750 m depth. The natural logarithm of this maximum concentration of DFe (750 m depth) versus the distance into the Nansen basin (Station 285–302), results in the following equation:

$$\mathrm{LnDFe} = -0.0038 \times \text{distance (km)} + 0.27, \quad (1)$$

where $R^2 = 0.97$, $n = 6$, and $P < 0.01$.

[27] Beyond station 302, no elevated values were observed at 750 m depth. From equation (1), we can calculate a scale length (defined as the distance to reduce the dissolved iron to 37% (1/e) of the initial concentration [*Johnson et al.*, 1997]) of 263 km. *Johnson et al.* [1997] reported a scale length of 5000 km at 1000 m depth in the east Pacific, off the coast of California. However, the strong scavenging regime and the fact that the currents in the Nansen Basin are along rather than perpendicular to the shelf (Figure 1b) can explain the order of magnitude difference in offshore transport of shelf derived DFe between the Nansen Basin and the east Pacific, where conditions for advective transport are more favorable [*Johnson et al.*, 1997]. *Laës et al.* [2007] observed that elevated Fe concentrations above the shelf, were not present ~147 km into the North Atlantic Ocean, confirming that the long distance transport of sediment derived DFe is strongly dependent on scavenging and advective transport by currents [*Laës et al.*, 2003, 2007].

[28] More to the east, toward the Laptev Sea shelf, a maximum in DFe concentration was observed at 300 m, together with a turbidity maximum (Figure 3c). Because of the correspondance of DFe with particle load and the fact that this maximum is ~700 m above the seafloor we suggest that that the elevated DFe at this station is caused by advective transport from the Laptev Sea shelf. The shallow (~50 m) Laptev Sea contains a large amount of particles and a high DFe (1.5–10 nM) [*Klunder et al.*, 2011] and TDFe (~20–40 nM) concentrations (P. Laan et al., unpublished data, 2008). Lower in the water column, at ~850 m, a turbidity and salinity maximum indicates the inflow of Atlantic water, possibly explained by the small fraction of Atlantic water coming through the Vilkitskij Strait, as reported by *Aksenov et al.* [2010]. Unfortunately, no DFe data is available for this depth, however, it is visible as a small enrichment at 900 m depth at station 389 (Figure 4).

#### 5.1.4. Fe Input From Hydrothermal Origin

[29] Hydrothermal vents are known to be an important source for iron in deep waters in the world ocean [*Klinkhammer et al.*, 2001; *Tagliabue et al.*, 2010]. *Edmonds et al.* [2003] reported active hydrothermal vents in the Arctic; the most eastern vent was located at (85°39′N, 84°50′E), approximately 60 km from our station 306 (Figure 1a). Indeed, elevated DFe concentrations were observed at a depth of 2000–3000 m in a large part of the Nansen and Amundsen Basins, and less pronounced, in the Makarov Basin (Figure 6). The highest DFe concentrations were observed at station 306, suggesting that this station is located closest to the hydrothermal input source. Moreover, at this station between 2000 and 3000 m depth, *Middag et al.* [2011] observed over ten-fold higher DMn compared to background concentrations and anomalies in light transmission and temperature confirming the presence of a hydrothermal vent source. Consistent with observations from the Southern Ocean [*Klunder et al.*, 2011], hydrothermal enrichment in DMn and DFe but no enrichment in dissolved Aluminum (DAl) was observed in the Arctic Deep Waters [*Middag et al.*, 2009, 2011].

[30] Based on a one dimensional scavenging model of *Craig* [1974], *Weiss* [1977] proposed an equation for removal of DMn with distance from a hydrothermal vent source. Applying this idea to DFe, for the special case where the currents are neglected ($v = 0$) this equation is

$$C = C_0 e^{-Ax}, \quad (2)$$

where $C$ is the concentration of DFe from the (hydrothermal) source (nM), $C_o$ is the initial concentration of DFe close the source (nM), $x$ is the distance to the source (cm), and $A = \sqrt{[K_h^{-1} \times \tau^{-1}]}$ ($K_h = 5 \times 10^6$ cm$^2$/s [*Weiss*, 1977] and $\tau$ = residence time (s)).

[31] Shown in Figure 10 are the DFe maxima at ~2250–2750 m versus the distance, for the stations, of transect 3 and transect 1 and 2 combined (only Nansen Basin stations). Also shown in Figure 10 are the calculated DFe concentrations with

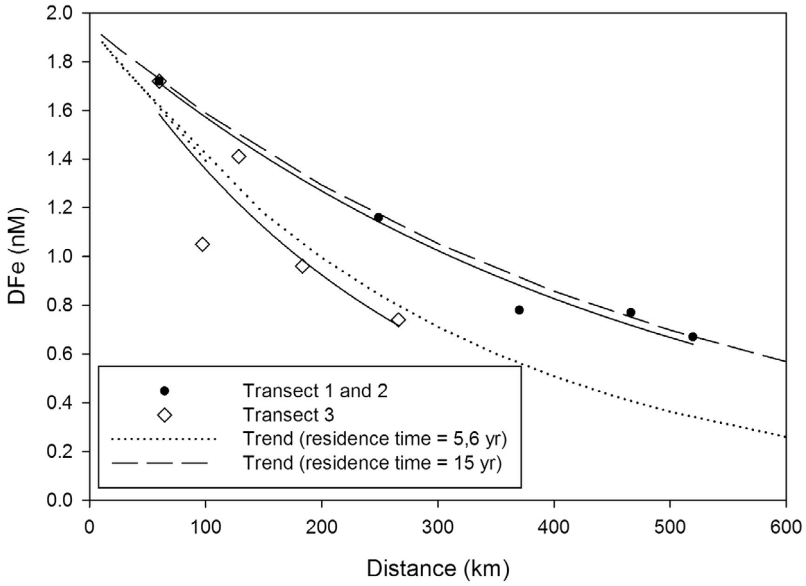


**Figure 10.** Trend of DFe (nM) with distance at the 2000–3000 m hydrothermal maximum in the Nansen Basin. Also shown is the calculated trend with distance using equation (2) (see text) and the residence time of 5,6 year [after *Moore and Braucher*, 2008] and 15 year [after *de Baar and de Jong*, 2001].

distance, based on a residence time of 5.6 years (reported for deep waters with strong scavenging regime by *Moore and Braucher* [2008]) and on a residence time of 15 years (lower end of range of *de Baar and de Jong* [2001]). The value for $C_0 = 1.95$ nM (calculated from the fit of transect 3 and transect 1 and 2) (equation (2)).

[32] For transect 1 and 2, a higher DFe-concentration relative to distance is observed. The best fit of these stations gives a residence time of 14.4 years, close to the model for a residence time of 15 years. For the parallel decreasing trend of dissolved Mn a much shorter residence time of 2 years was reported [*Middag et al.*, 2011]. In contrast the stations of transect 3 show a lower DFe with distance, and the best fit gives a shorter 4.7 year residence time. For the parallel decreasing trend of dissolved Mn again a shorter residence time of 0.4 year was reported [*Middag et al.*, 2011].

[33] The relatively more rapid loss of Mn versus Fe is in contrast with previous observations, for much higher concentrations, very close to the hydrothermal source. For the Juan de Fuca Ridge, *Field and Sherrell* [2000] report a trend of DFe from 319 to 20 nM over the short distance of 3.7 km from the vent source, versus an apparent trend of DMn from 193 to 27 nM. By implicitly assuming that the latter Mn trend is merely due to dilution, for DFe an apparent oxidation half-life of ~3.33 h was derived. Latter more rapid loss of Fe versus Mn is in keeping with the generally more rapid inorganic oxidation of Fe versus Mn [*Cowen et al.*, 1990].

[34] The key difference between our observations at low concentrations and long distances, and the high concentrations and short distances over the Juan de Fuca ridge, is in the natural organic complexation of Fe in ocean waters. Briefly there is a general background level of organic Fe-binding ligand of 1.98–2.05 nM observed in the same samples over Gakkel Ridge [*Thuróczy et al.*, 2011]. Such Fe-binding ligand concentrations are typical throughout the world oceans. When the DFe concentration is near this ligand concentration, most of the DFe is stabilized in solution thus preventing scavenging loss. In contrast dissolved Mn is not organically complexed, hence will be scavenged more rapidly. At the very high DFe in the 20–319 nM range over Juan de Fuca ridge, the low ~2nM ligand concentration is inadequate, the large majority of dissolved Fe is inorganic, hence will be rapidly scavenged.

[35] The difference in residence time observed for transect 1–2, and transect 3 is not expected within a uniform basin. The difference in DFe decrease may also be caused by the flow direction in the deep Arctic Ocean. *Weiss* [1977] showed a strong effect of velocity in removal with distance; a positively directed flow ($v > 0$; from the vent toward the location of the stations) would cause a higher concentration for the same distance compared to the modeled fit (where $v = 0$ is assumed). Based on the flow patterns (Figure 1b), a positive flow is expected toward transect 1 and 2, whereas toward transect 3, more perpendicular to the currents, the direction is 0 or even slightly negative (Figure 1b). Although the data does not provide a definite conclusion, it seems likely that the different decrease patterns of DFe with depth are related rather to flow patterns than to a (large) difference in residence time. To the best of our knowledge, there is no data on specific residence times of DFe with respect to hydrothermal input. Nevertheless, the fact that the residence time is between the range of 15–41 yr published by *de Baar and de Jong* [2001] for the deep oceans worldwide and the 5.6 yr published for deep oceans with a high scavenging regime by *Moore and Braucher* [2008] supports a strong scavenging regime in the deep Nansen Basin.

[36] Hydrothermal vents are also reported at ~37° (~3200 m) and ~43°E (depth unknown) [*Edmonds et al.*, 2003] (Figure 1b). With the general northwest flow direction, transect 1 was situated downstream of the flow direction whereas transect 2 was further away and upstream of the flow direction (Figure 1b) [*Rudels*, 2001]. In the northwestern

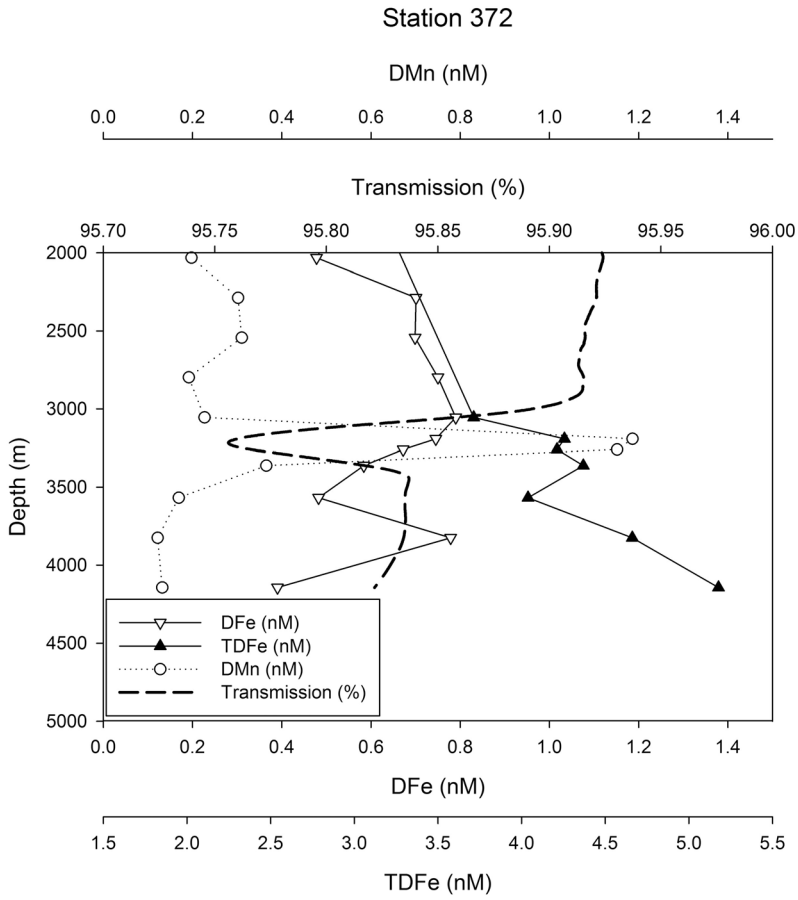


**Figure 11.** Dissolved Fe (DFe, nM), total Fe (TFe, nM), dissolved Mn (DMn, nM) and transmission signal (%) (smoothed) for station 372, indicative of a hydrothermal plume.

Nansen Basin, station 260 showed the strongest concentration increase of >1 nM DFe at 2000–3000 m depth, whereas stations more to the east (station 261) (Figure 5) and south (station 258) (Figure 2) show separate DFe maxima (of ~0.1 nM above background) at ~2200–2600 and ~3200 m. However, the strong DFe maximum at station 260 may also be caused by two separate DFe-enrichments, as was observed in the Mn signal [*Middag et al.*, 2011]. The fact that this is the strongest signal, indicates that the hydrothermal plume which causes the DFe enrichment at 3200 m likely came from the north(-east) direction. Therefore we suggest that the elevated DFe concentration at ~3200 m originates from the hydrothermal vents at 37° and/or ~43°E as reported by *Edmonds et al.* [2003].

[37] Above the east part of the Gakkel Ridge, from ~103°E (stations 371–373), the hydrothermal signal at ~2500 m was not very pronounced in the DFe (Figure 8). However, a signal was observed in the light transmission, temperature and DFe profiles at ~3000–3500 m (Figure 11). At station 372 (and 373) also total dissolvable Fe (TDFe) was measured at high resolution below 2000 m depth as shown in Figure 11. Although there are elevated concentrations of dissolved Fe over a broad depth range from 2200 to 3600 m depth, there is a local, stronger, maximum of total Fe (TDFe) at 3200–3360 m (Figure 11). The stronger increase in TDFe relative to DFe in hydrothermal influenced waters is also reported by *Boyle et al.* [2005]. These findings are coincident with increase in dissolved manganese and a local increase in $\theta$ are observed at station 372, at a depth of 3100–3300 m [*Middag et al.*, 2011].

[38] At station 372, a geostrophic velocity (relative to 3000 m depth) of close to 0 is observed, possibly preventing mixing of a hydrothermal source with waters above and below. In contrast, at stations 371 and 373 stronger velocities are observed (data not shown), possibly causing mixing of a hydrothermal source with surrounding waters.

[39] The increase in concentration in the hydrothermal plume is relatively low at station 372 compared to that at station 306 both for DFe and DMn [*Middag et al.*, 2011]. The vents described by *Edmonds et al.* [2003] are all situated west of 84°E (Figure 1) and to the best of our knowledge there is no vent discovered east of 85°E. The fact that the signal is only observed at station 372, may imply that the source of the hydrothermal signal observed at station 372 comes from a thus far undiscovered vent in this region. Alternatively, the signal could be transported to the region of station 372 from further east. A strong hydrothermal source is observed at ~3200 m depth at 37°E [*Edmonds et al.*, 2003] (Figure 1a), which is situated slightly north of the rift valley, i.e., on the Amundsen Basin side of the ridge. Although the flow direction for water in the deep Amundsen Basin is westward [*Rudels*, 2001], an eastward return flow was proposed by *Jones et al.* [1995] for waters below 2000 m water in the Amundsen basin, which may explain

**Table 1.** $DFe/NO_3^-$ Three Ratios and DFe Concentrations in the Deep Waters in the Different Basins[a]

| | Basin | | |
|---|---|---|---|
| | Nansen | Amundsen | Makarov |
| Water mass | DEBW | DEBW | DMBW |
| $DFe/NO_3^-$ | | | |
| Average | 0.047 | 0.031 | 0.026 |
| Standard deviation | 0.017 | 0.007 | 0.013 |
| $n$[b] | 154 | 28 | 52 |
| $P$[c] | | <0.05 | <0.05 |
| Decrease (%) | | 33% | 16% |
| DFe (nM) | | | |
| Average | 0.70 | 0.47 | 0.39 |
| Standard deviation | 0.25 | 0.11 | 0.19 |
| $n$[b] | 157 | 28 | 52 |
| $P$[c] | | <0.05 | <0.05 |

[a]DEBW, Deep Eurasian Basin Water; DMBW, Deep Makarov Basin Water.
[b]For three stations in the Nansen Basin there is no $NO_3^-$ data available.
[c]Two-sided heteroscedastic T-test.

the observation of the elevated DFe signal so far from the source.

#### 5.1.5. Fe in the Deep Waters: Deep Remineralization, Scavenging and Organic Complexation

[40] Generally, in the deep waters of the world ocean the distribution of DFe is determined by an interplay of (passive) particle scavenging of iron from the dissolved phase [*Johnson et al.*, 1997] and organic complexation [*Wu and Luther*, 1995; *Wu et al.*, 2001]. The DFe distribution is also affected by the remineralization of biogenic particles [*Martin and Gordon*, 1988; *Sunda and Huntsman*, 1995]. The distribution of nitrate ($NO_3^-$) throughout the water column is determined by the process of biological uptake and remineralization and not by scavenging [*Murray*, 1992]. Therefore, the $DFe/NO_3$ ratio can give an indication of the relative importance of the scavenging regime (and complexation). For example, *Sarthou et al.* [2007] showed lower values of the $DFe/NO_3^-$ ratio were consistent with a stronger scavenging regime in the North Atlantic Ocean. In Table 1 the average $DFe/NO_3^-$ ratios and DFe concentrations are shown for the deep waters (EBDW, MBDW) in the Nansen, Amundsen and Makarov Basin respectively. There is a significant difference in $DFe/NO_3$ between the Nansen and Amundsen Basins (~33%). *Parekh et al.* [2005] showed in a model study that decreasing the scavenging ratio by 40% results in a ~0.1 nM increase in DFe in the deep global oceans. Scavenging removal of DFe is reported for all Arctic Basins [*Thuróczy et al.*, 2011]. The difference in DFe between the Nansen and Amundsen Basins is 0.23 nM (Table 1), significantly larger than the difference in scavenging removal that would be expected on the basis of the $DFe/NO_3$ – ratio and the model results of *Parekh et al.* [2005]. Possible explanations for this discrepancy are (1) larger input flux of DFe in the EBDW in the Nansen Basin or (2) lower or less strong organic complexation (resulting in more scavenging removal) in the Amundsen Basin compared to the Nansen Basin or a combination of both factors.

[41] As discussed above (sections 5.1.2 and 5.1.4), there are strong input sources in the Nansen Basin, i.e., DFe input from the slope and hydrothermal DFe input. We argue that the difference in DFe between the Nansen Basin and Amundsen Basin can be attributed mainly to the larger Fe input flux in the deep Nansen Basin, which is also consistent with the Al and Ba data (see section 5.1.2), rather than to differences in organic complexation. The organic complexation and size fractionation of Fe is described by *Thuróczy et al.* [2011]. Briefly, for the size fraction <0.2 $\mu$m, ranges of ligand concentrations (equation of nM), binding strengths (-) and ligand saturation (Excess L/Fe) are $1.82 \pm 0.33$, $22.01 \pm 0.15$, and $1.46 \pm 0.44$ for the EBDW in the Nansen Basin. The values for the Amundsen Basin are $1.57 \pm 0.50$, $21.59 \pm 0.37$, and $3.41 \pm 0.6$ respectively. In general, the fact that there is a higher reactivity yet lower saturation state of the ligands in the Nansen compared to the Amundsen Basin make that the difference in organic complexation is difficult to quantify [*Thuróczy et al.*, 2011]. We argue that the difference in DFe between the Nansen Basin and Amundsen Basin can be attributed mainly to the larger Fe input flux in the deep Nansen Basin, which is also consistent with the Al and Ba data (see section 5.1.2), rather than to differences in organic complexation.

[42] Between the Amundsen and Makarov Basin there is only a small decrease in the $DFe/NO_3^-$ ratio, which is consistent with the small decrease in DFe between both Basins (Table 1). Canada Basin Deep Water is relatively old compared to Eurasian Basin Deep Water as the latter water mass is stronger affected by downslope convection [*Rudels*, 2001]. Therefore, the scavenging removal may have been going on for a longer time in the Makarov Basin. Moreover, in the Amundsen Basin hydrothermally originated DFe is present (Figure 6), whereas this input source is very small for the Makarov Basin. The DFe scavenging removal as a consequence of lower reactivity of ligands in the Makarov Basin will lead to a little saturated ligands. Ligand characteristics (ligand concentration, binding strength and saturation) are $1.35 \pm 39$, $21.64 \pm 0.13$, and $4.66 \pm 0.45$ respectively [*Thuróczy et al.*, 2011]. Therefore, we suggest that the difference in DFe input and in age between these water masses are the main factors controlling the DFe concentration.

[43] To take a closer look at the importance of input fluxes relative to scavenging removal in the distribution of DFe we look at the relationship between DFe an DMn in the deep water masses. The formula for scavenging removal is

$$S_c = k[Me]C_p, \tag{3}$$

where $S_c$ is the scavenging rate removal (nM $d^{-1}$), $k$ is the scavenging rate ($d^{-1}$), $[Me]$ is the concentration of the metal (nM), and $C_p$ = the concentration of particles (-).

[44] The behavior of DMn is similar to that of DFe. Therefore if the dominant process in the deep Arctic Ocean is scavenging, the relation of both metals is to be expected to be of the form DMn = (aDFe)/b with $a = S_{c\,Mn}k_{Fe}$ and $b = S_{c\,Fe}k_{Mn}$ (derived from equation (3)). In the deeper waters (>3000 m) of the Amundsen and Makarov Basins (Figure 12), such a relation was observed, with $R^2 = 0.74$ ($n = 27$). Here, the "external" Fe-input was very low, and therefore scavenging removal likely is the dominant process. Higher in the water column, and in the Nansen Basin, there are more factors, such as hydrothermal and slope input, influencing the DFe and DMn distribution in all

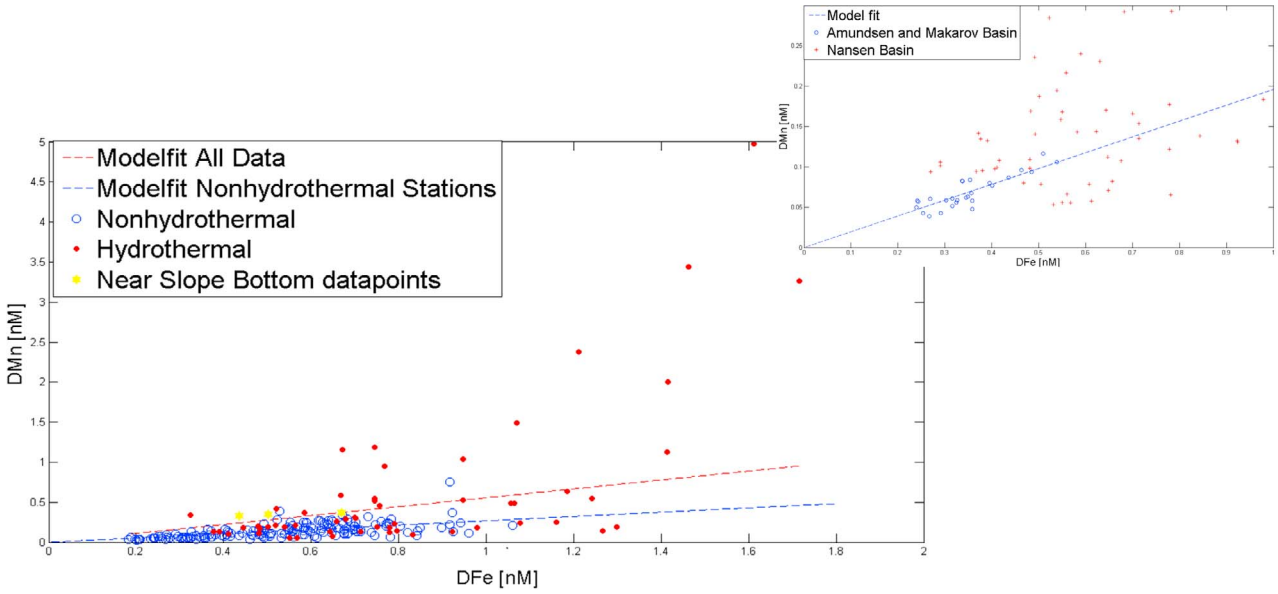


**Figure 12.** Relationship between DFe (nM) and DMn (nM) for all data points within the DMBW and DEBW (see text). Stations indicated with "hydrothermal" are stations 260, 261, 301–306, and 372. Inset of Figure 12 at expanded scale: Relationship between DFe (nM) and DMn (nM) for all data points >3000 m. Makarov and Amundsen data points show a correlation: [DMn] (nM) = (0.15[DFe] (nM))/ 0.75 with ($R^2$ = 0.74, $n$ = 27).

Arctic Basins, leading to a disappearance of the DFe, DMn - relationship (Figure 12). Enrichment in DMn compared to DFe is observed in the stations qualified as "hydrothermal." However, some data points in the Nansen Basin show relatively higher DFe compared to DMn (Figure 12). A possible explanation may be that these waters are part of a deep counter current as proposed by *Jones et al.* [1995]. The long transit time from the vents (situated more to the east) would then remove DMn relatively fast compared to DFe, resulting in the observed a relatively low DMn compared to DFe. The deepest, near-bottom data points of the stations 255, 363, and 389 situated above continental and Mendeleev Ridge slope regions appear to be enriched in DMn, which may be derived from recent resuspension of slope sediment [*Middag et al.*, 2011].

### 5.2. Implications for the DFe Cycle in the Deep Arctic Ocean

[45] Recently, *Moore and Braucher* [2008] compiled the available data and presented (averaged) depth profiles of DFe concentration in three world ocean regions (North Atlantic, North Pacific, and Southern Ocean). In Figure 9 similar plots for the Arctic Basins are shown (in the Nansen Basin discrimination is made between the east and west part of the Basin) along with the profiles of *Moore and Braucher* [2008], updated with recent DFe data (M. Rijkenberg and P. Laan, unpublished data, 2011). There are clear interbasin deviations in the DFe concentrations; a relatively high (∼0.7 nM) concentration of DFe at 500–1500 m depth in the west part of the Nansen Basin compared to the east part and an even greater difference compared to the Amundsen and Makarov Basins, is likely caused by inflow of North Atlantic Water (see section 5.1.1). In general, in the upper 2000 m the concentrations decrease from the Siberian shelf to the Canadian side, with highest concentrations in the Nansen Basin and lowest in the Makarov Basin. Also shown are recent DFe concentrations from the Canada Basin (only Slope and Basin stations included (B1–B3)), close to the Chuckchi plateau (150–160°W,∼75°N) [*Nakayama et al.*, 2011]. The high concentrations in the upper depth interval (250–500) may be caused by intense remineralisation (as also confirmed by AOU and nutrients) [*Nakayama et al.*, 2011]. Below, DFe gradually declines and deep water concentrations are ∼0.1 nM higher than those in the Makarov Basin, which could be attributed to slope influence (stations located nearby the slope) and to strong remineralisation, causing higher DFe at depth. No enrichment at ∼2000 m depth is observed in this part of the Canada Basin. Moreover, the DFe distribution in the Arctic Ocean, particularly in the Makarov Basin, shows some deviation from the distribution in other regions of the world ocean (Figure 9). First of all, although dissolved Fe concentrations in the upper layers in the Arctic can be high (>2 nM) [*Klunder et al.*, 2011] the concentrations decrease readily with depth. The strong stratification largely prevents mixing between the deep waters and the surface waters [*Rudels*, 2001]. Second, the hydrothermal input is clearly visible in the Nansen and Amundsen Basins, resulting in a pronounced maximum in DFe at ∼2500 m, which is not present in the North Atlantic (maximum at 1000–1500 m) and North Pacific (broad maximum (1000–3000 m). The hydrothermal maximum is absent in the Makarov Basin. Below this maximum, scavenging is the controlling factor and DFe concentrations decrease with depth, as also observed in other world oceans (Figure 9). Third, in the Makarov Basin, the absence of input sources and the fact that the water is relatively old, cannot be (fully) compensated by organic complexation leading to a strong

scavenging removal and very low DFe concentrations (~0.25 nM).

## 6. Summary and Conclusions

[46] The distribution of dissolved Fe in the deep waters of the Arctic Ocean deviates from that in all other regions of the world ocean. Moreover, there are strong differences between the different Arctic Ocean Basins. Over the whole Arctic Ocean, strong stratification largely prevents mixing between the deep water concentrations and the surface waters in the Arctic Ocean. However, DFe is transported from the shelf seas to the Arctic Deep waters, mainly by downslope convection and re-suspension of sediment from the slopes. The Atlantic Ocean is the main source of water to the Arctic, which is reflected in the higher Fe concentrations in the (western) Nansen Basin at intermediate depths. Remineralization of Fe from biogenic particles appears to have a relatively low impact on deep water DFe concentrations. This may be due to a low POC export from the surface, in combination with a strong scavenging regime, which enhances fast settling. The hydrothermal input source above the Gakkel ridge causes DFe enrichment at a depth of 2000–3000 m depth in most of the central Arctic Ocean. Below this depth layer, scavenging plays an important role in the deep waters, whereas the effect of organic complexation is relatively weak; concentrations decrease rapidly and reach very low values in the deep Makarov and Amundsen Basins. The high DFe concentration in the shelf waters flowing in the Central Arctic ((mainly) river derived [*Klunder et al.*, 2011]), and hydrothermal enrichment of DFe to the Arctic Ocean will give a net addition of DFe to the marine environment. Upwelling of these waters [*Yang*, 2009] may cause relatively high DFe concentrations in the PSW and intermediate waters, and eventually in the return flow to the North Atlantic Ocean.

[47] **Acknowledgments.** The authors want to thank captain S. Schwarze and his crew of the RV *Polarstern*. Lorendz Boom and Sven Ober are gratefully acknowledged for technical assistance. The authors thank Micha Rijkenberg and two anonymous reviewers for their constructive comments.

## References

Aguilar-Islas, A. M., M. P. Hurst, K. N. Buck, B. Sohst, G. J. Smith, M. C. Lohan, and K. W. Bruland (2007), Micro- and macronutrients in the southeastern Bering Sea: Insight into iron-replete and iron-depleted regimes, *Prog. Oceanogr.*, *73*, 99–126, doi:10.1016/j.pocean.2006.12.002.

Aguilar-Islas, A. M., R. D. Rember, C. W. Mordy, and J. Wu (2008), Sea ice-derived dissolved iron and its potential influence on the spring algal bloom in the Bering Sea, *Geophys. Res. Lett.*, *35*, L24601, doi:10.1029/2008GL035736.

Aksenov, Y., S. Bacon, A. C. Coward, and A. J. G. Nurser (2010), The North Atlantic inflow to the Arctic Ocean, *J. Mar. Syst.*, *79*(1–2), 1–22, doi:10.1016/j.jmarsys.2009.05.003.

Anderson, L. G., E. P. Jones, and J. H. Swift (2003), Export production in the central Arctic Ocean evaluated from phosphate deficits, *J. Geophys. Res.*, *108*(C6), 3199, doi:10.1029/2001JC001057.

Ardelan, M. V., O. Holm-Hansen, C. D. Hewes, C. S. Reiss, N. S. Silva, H. Dulaiova, E. Steinnes, and E. Sakshaug (2010), Natural iron enrichment around the Antarctic Peninsula in the Southern Ocean, *Biogeosciences*, *7*(1), 11–25, doi:10.5194/bg-7-11-2010.

Arrigo, K. R., G. van Dijken, and S. Pabi (2008), Impact of a shrinking Arctic ice cover on marine primary production, *Geophys. Res. Lett.*, *35*, L19603, doi:10.1029/2008GL035028.

Boyd, P. W., et al. (2000), A mesoscale phytoplankton bloom in the polar Southern Ocean stimulated by iron fertilization, *Nature*, *407*, 695–702, doi:10.1038/35037500.

Boyle, E. A., B. A. Bergquist, R. A. Kayser, and N. Mahowald (2005), Iron, manganese, and lead at Hawaii Ocean Time-Series station ALOHA: Temporal variability and an intermediate water hydrothermal plume, *Geochim. Cosmochim. Acta*, *69*(4), 933–952, doi:10.1016/j.gca.2004.07.034.

Bruland, K. W., N. M. Price, and M. L. Wells (1995), Iron chemistry in seawater and its relationship to phytoplankton: A workshop report, *Mar. Chem.*, *48*(1), 157–182.

Bucciarelli, E., S. Blain, and P. Tréguer (2001), Iron and manganese in the wake of the Kerguelen Islands (Southern Ocean), *Mar. Chem.*, *73*(1), 21–36, doi:10.1016/S0304-4203(00)00070-0.

Cai, P., M. Rutgers van der Loeff, I. Stimac, E. M. Nöthig, K. Lepore, and S. B. Moran (2010), Low export flux of particulate organic carbon in the central Arctic Ocean as revealed by $^{234}Th$:$^{238}U$ disequilibrium, *J. Geophys. Res.*, *115*, C10037, doi:10.1029/2009JC005595.

Campbell, J. A., and P. A. Yeats (1982), The distribution of manganese, iron, nickel, copper and cadmium in the waters of Baffin Bay and the Canadian Arctic Archipelago, *Oceanol. Acta*, *5*(2), 161–168.

Chever, F., E. Bucciarelli, G. Sarthou, S. Speich, M. Arhan, P. Penven, and A. Tagliabue (2010), Physical speciation of iron in the Atlantic sector of the Southern Ocean along a transect from the subtropical domain to the Weddell Sea Gyre, *J. Geophys. Res.*, *115*, C10059, doi:10.1029/2009JC005880.

Cowen, J. P., G. P. Massoth, and R. A. Feely (1990), Scavenging rates of dissolved manganese in a hydrothermal vent plume, *Deep Sea Res., Part A*, *37*(10), 1619–1637, doi:10.1016/0198-0149(90)90065-4.

Craig, H. (1974), A scavenging model for trace elements in the deep sea, *Earth Planet. Sci. Lett.*, *23*(1), 149–159, doi:10.1016/0012-821X(74)90042-9.

Croot, P. L., and K. A. Hunter (1998), Trace metal distributions across the continental shelf near Otago Peninsula, New Zealand, *Mar. Chem.*, *62*(3–4), 185–201, doi:10.1016/S0304-4203(98)00036-X.

D'Asaro, E. A., and J. H. Morison (1992), Internal waves and mixing in the Arctic Ocean, *Deep Sea Res., Part A*, *39*(2), S459–S484, doi:10.1016/S0198-0149(06)80016-6.

de Baar, H. J. W., and J. T. M. de Jong (2001), Distributions, sources and sinks of iron in seawater, in *The Biogeochemistry of Iron in Seawater*, *Ser. Anal. Phys. Chem. Environ. Syst.*, vol. 7, edited by D. R. Turner and K. A. Hunter, chap. 5, pp. 123–254, Wiley, Chichester, U. K.

de Baar, H. J. W., J. T. M. de Jong, D. C. E. Bakker, B. M. Löscher, C. Veth, U. Bathmann, and V. Smetacek (1995), Importance of iron for phytoplankton blooms and carbon dioxide drawdown in the Southern Ocean, *Nature*, *373*, 412–415, doi:10.1038/373412a0.

de Baar, H. J. W., et al. (2008), Titan: A new facility for ultraclean sampling of trace elements and isotopes in the deep oceans in the international Geotraces program, *Mar. Chem.*, *111*(1–2), 4–21, doi:10.1016/j.marchem.2007.07.009.

Edmonds, H. N., P. J. Michael, E. T. Baker, D. P. Connelly, J. E. Snow, C. H. Langmuir, H. J. B. Dick, R. Muhe, C. R. German, and D. W. Graham (2003), Discovery of abundant hydrothermal venting on the ultraslow-spreading Gakkel ridge in the Arctic Ocean, *Nature*, *421*(6920), 252–256, doi:10.1038/nature01351.

Ekwurzel, B., P. Schlosser, R. A. Mortlock, R. G. Fairbanks, and J. H. Swift (2001), River runoff, sea ice meltwater, and Pacific water distribution and mean residence times in the Arctic Ocean, *J. Geophys. Res.*, *106*(C5), 9075–9092, doi:10.1029/1999JC000024.

Elrod, V. A., W. H. Berelson, K. H. Coale, and K. S. Johnson (2004), The flux of iron from continental shelf sediments: A missing source for global budgets, *Geophys. Res. Lett.*, *31*, L12307, doi:10.1029/2004GL020216.

Fahl, K., and E.-M. Nöthig (2007), Lithogenic and biogenic particle fluxes on the Lomonosov Ridge (central Arctic Ocean) and their relevance for sediment accumulation: Vertical vs. lateral transport, *Deep Sea Res., Part I*, *54*(8), 1256–1272, doi:10.1016/j.dsr.2007.04.014.

Field, M. P., and R. M. Sherrell (2000), Dissolved and particulate Fe in a hydrothermal plume at 9°45′N, East Pacific Rise: Slow Fe(II) oxidation kinetics in Pacific plumes, *Geochim. Cosmo. Acta*, *64*(4), 619–628, doi:10.1016/S0016-7037(99)00333-6.

Gregg, W. W., M. E. Conkright, P. Ginoux, J. E. O'Reilly, and N. W. Casey (2003), Ocean primary production and climate: Global decadal changes, *Geophys. Res. Lett.*, *30*(15), 1809, doi:10.1029/2003GL016889.

Johnson, K. S., R. M. Gordon, and K. H. Coale (1997), What controls dissolved iron concentrations in the world ocean?, *Mar. Chem.*, *57*(3–4), 137–161, doi:10.1016/S0304-4203(97)00043-1.

Jones, E. P., B. Rudels, and L. G. Anderson (1995), Deep waters of the Arctic Ocean: Origins and circulation, *Deep Sea Res., Part I*, *42*(5), 737–760, doi:10.1016/0967-0637(95)00013-V.

Klinkhammer, G. P., C. S. Chin, R. A. Keller, A. Dählmann, H. Sahling, G. Sarthou, S. Petersen, F. Smith, and C. Wilson (2001), Discovery of new hydrothermal vent sites in Bransfield Strait, Antarctica, *Earth Planet. Sci. Lett.*, *193*(3–4), 395–407, doi:10.1016/S0012-821X(01)00536-2.

Klunder, M. B., P. Laan, R. Middag, H. J. W. de Baar, and J. C. van Ooijen (2011), Dissolved iron in the Southern Ocean (Atlantic sector), *Deep Sea Res., Part II*, *58*, 2678–2694.

Klunder, M. B., D. Bauch, P. Laan, H. J. W. de Baar, S. van Heuven, and S. Ober (2012), Dissolved iron in the Arctic shelf seas and surface waters of the central Arctic Ocean: Impact of Arctic river water and ice-melt, *J. Geophys. Res.*, *117*, C01027, doi:10.1029/2011JC007133.

Laës, A., S. Blain, P. Laan, E. P. Achterberg, G. Sarthou, and H. J. W. de Baar (2003), Deep dissolved iron profiles in the eastern North Atlantic in relation to water masses, *Geophys. Res. Lett.*, *30*(17), 1902, doi:10.1029/2003GL017902.

Laës, A., S. Blain, P. Laan, S. J. Ussher, E. P. Achterberg, P. Tréguer, and H. J. W. de Baar (2007), Sources and transport of dissolved iron and manganese along the continental margin of the Bay of Biscay, *Biogeosciences*, *4*(2), 181–194, doi:10.5194/bg-4-181-2007.

Lam, P. J., and J. K. B. Bishop (2008), The continental margin is a key source of iron to the HNLC North Pacific Ocean, *Geophys. Res. Lett.*, *35*, L07608, doi:10.1029/2008GL033294.

Martin, J. H., and R. M. Gordon (1988), Northeast Pacific iron distributions in relation to phytoplankton productivity, *Deep Sea Res., Part A*, *35*(2), 177–196, doi:10.1016/0198-0149(88)90035-0.

Measures, C. I. (1999), The role of entrained sediments in sea ice in the distribution of aluminium and iron in the surface waters of the Arctic Ocean, *Mar. Chem.*, *68*(1–2), 59–70, doi:10.1016/S0304-4203(99)00065-1.

Middag, R. (2010), Dissolved aluminium and manganese in the polar oceans, PhD thesis, Rijksuniv. Groningen, Groningen, Netherlands.

Middag, R., H. J. W. de Baar, P. Laan, and K. Bakker (2009), Dissolved aluminium and the silicon cycle in the Arctic Ocean, *Mar. Chem.*, *115*(3–4), 176–195, doi:10.1016/j.marchem.2009.08.002.

Middag, R., H. J. W. de Baar, P. Laan, and M. B. Klunder (2011), Fluvial and hydrothermal input of manganese into the Arctic Ocean, *Geochim. Cosmochim. Acta*, *75*(9), 2393–2408, doi:10.1016/j.gca.2011.02.011.

Moore, J. K., and O. Braucher (2008), Sedimentary and mineral dust sources of dissolved iron to the world ocean, *Biogeosciences*, *5*(3), 631–656, doi:10.5194/bg-5-631-2008.

Murray, J. W. (1992), The oceans, in *Global Biogeochemical Cycles*, *Int. Geophys. Ser.*, vol. 50, edited by S. S. Butcher et al., chap. 4, pp. 175–211, Academic, London, doi:10.1016/S0074-6142(08)62692-3.

Nakayama, Y., S. Fujita, K. Kuma, and K. Shimada (2011), Iron and humic-type fluorescent dissolved organic matter in the Chukchi Sea and Canada Basin of the western Arctic Ocean, *J. Geophys. Res.*, *116*, C07031, doi:10.1029/2010JC006779.

Parekh, P., M. J. Follows, and E. Boyle (2004), Modeling the global ocean iron cycle, *Global Biogeochem. Cycles*, *18*, GB1002, doi:10.1029/2003GB002061.

Parekh, P., M. J. Follows, and E. A. Boyle (2005), Decoupling of iron and phosphate in the global ocean, *Global Biogeochem. Cycles*, *19*, GB2020, doi:10.1029/2004GB002280.

Roeske, T., M. Rutgers vd Loeff, R. Middag, and K. Bakker (2012), Deep water circulation and composition in the Arctic Ocean by dissolved barium, aluminium and silicate, *Mar. Chem.*, *132-133*, 56–67, doi:10.1016/j.marchem.2012.02.001.

Rudels, B. (2001), Arctic Basin circulation, in *Encyclopedia of Ocean Sciences*, edited by J. H. Steele, S. A. Thorpe, and K. K. Turekian, pp. 177–187, Academic, San Diego, Calif., doi:10.1006/rwos.2001.0372.

Rudels, B., R. D. Muench, J. Gunn, U. Schauer, and H. J. Friedrich (2000), Evolution of the Arctic Ocean boundary current north of the Siberian shelves, *J. Mar. Syst.*, *25*(1), 77–99, doi:10.1016/S0924-7963(00)00009-9.

Rudels, B., G. Björk, J. Nilsson, P. Winsor, I. Lake, and C. Nohr (2005), The interaction between waters from the Arctic Ocean and the Nordic Seas north of Fram Strait and along the East Greenland Current: Results from the Arctic Ocean-02 Oden expedition, *J. Mar. Syst.*, *55*(1–2), 1–30, doi:10.1016/j.jmarsys.2004.06.008.

Sarthou, G., A. R. Baker, J. Kramer, P. Laan, A. Laës, S. Ussher, E. P. Achterberg, H. J. W. de Baar, K. R. Timmermans, and S. Blain (2007), Influence of atmospheric inputs on the iron distribution in the subtropical north-east Atlantic Ocean, *Mar. Chem.*, *104*(3–4), 186–202, doi:10.1016/j.marchem.2006.11.004.

Schauer, U., R. D. Muench, B. Rudels, and L. Timokhov (1997), Impact of eastern Arctic shelf waters on the Nansen Basin intermediate layers, *J. Geophys. Res.*, *102*(C2), 3371–3382, doi:10.1029/96JC03366.

Schauer, U., H. Loeng, B. Rudels, V. K. Ozhigin, and W. Dieck (2002), Atlantic water flow through the Barents and Kara Seas, *Deep Sea Res., Part I*, *49*, 2281–2298, doi:10.1016/S0967-0637(02)00125-5.

Schlitzer, R. (2002), Ocean Data View, http://odv.awi.de/, Alfred Wegener Inst. for Polar and Mar. Res., Bremerhaven, Germany.

Sunda, W. G., and S. A. Huntsman (1995), Iron uptake and growth limitation in oceanic and coastal phytoplankton, *Mar. Chem.*, *50*(1–4), 189–206, doi:10.1016/0304-4203(95)00035-P.

Tagliabue, A., et al. (2010), Hydrothermal contribution to the oceanic dissolved iron inventory, *Nat. Geosci.*, *3*(4), 252–256, doi:10.1038/ngeo818.

Tanhua, T., K. A. Olsson, and E. Jeansson (2005), Formation of Denmark Strait overflow water and its hydro-chemical composition, *J. Mar. Syst.*, *57*(3–4), 264–288, doi:10.1016/j.jmarsys.2005.05.003.

Thuróczy, C.-E., L. J. A. Gerringa, M. Klunder, P. Laan, and H. J. W. de Baar (2011), Distinct trends in the speciation of iron between the shallow shelf seas and the deep basins of the Arctic Ocean, *J. Geophys. Res.*, *116*, C10009, doi:10.1029/2010JC006835.

Turner, D. R., and K. A. Hunter (Eds.) (2001), *The Biogeochemistry of Iron in Seawater*, *Ser. Anal. Phys. Chem. Environ. Syst.*, vol. 7, Wiley, Chichester, U. K.

Weiss, R. F. (1977), Hydrothermal manganese in the deep sea: Scavenging residence time and Mn/$^3$He relationships, *Earth Planet. Sci. Lett.*, *37*(2), 257–262, doi:10.1016/0012-821X(77)90171-6.

Wu, J., and G. W. Luther (1995), Complexation of Fe(III) by natural organic ligands in the northwest Atlantic Ocean by a competitive ligand equilibration method and a kinetic approach, *Mar. Chem.*, *50*(1–4), 159–177, doi:10.1016/0304-4203(95)00033-N.

Wu, J., E. Boyle, W. Sunda, and L.-S. Wen (2001), Soluble and colloidal iron in the oligotrophic North Atlantic and North Pacific, *Science*, *293*(5531), 847–849, doi:10.1126/science.1059251.

Wu, J., M. L. Wells, and R. Rember (2011), Dissolved iron anomaly in the deep tropical-subtropical Pacific: Evidence for long-range transport of hydrothermal iron, *Geochim. Cosmochim. Acta*, *75*(2), 460–468, doi:10.1016/j.gca.2010.10.024.

Yang, J. (2009), Seasonal and interannual variability of downwelling in the Beaufort Sea, *J. Geophys. Res.*, *114*, C00A14, doi:10.1029/2008JC005084.

K. Bakker, Geological Oceanography, Royal Netherlands Institute for Sea Research, Lansdiep 4, Den Burg NL-1797 SZ, Netherlands.

H. J. W. de Baar, M. B. Klunder, P. Laan, and R. Middag, Biological Oceanography, Royal Netherlands Institute for Sea Research, Landsdiep 4, Den Burg NL-1797 SZ, Netherlands. (maarten.klunder@nioz.nl)